Turbulent flame propagation in partially premixed flames

By T. Poinsot[1], D. Veynante[2], A. Trouvé[3] AND G. Ruetsch[4]

1. Introduction

Turbulent premixed flame propagation is essential in many practical devices. In the past, fundamental and modeling studies of propagating flames have generally focused on turbulent flame propagation in mixtures of homogeneous composition, *i.e.* a mixture where the fuel-oxidizer mass ratio, or equivalence ratio, is uniform. This situation corresponds to the ideal case of perfect premixing between fuel and oxidizer. In practical situations, however, deviations from this ideal case occur frequently. In stratified reciprocating engines, fuel injection and large-scale flow motions are fine-tuned to create a mean gradient of equivalence ratio in the combustion chamber which provides additional control on combustion performance. In aircraft engines, combustion occurs with fuel and secondary air injected at various locations resulting in a nonuniform equivalence ratio. In both examples, mean values of the equivalence ratio can exhibit strong spatial and temporal variations. These variations in mixture composition are particularly significant in engines that use direct fuel injection into the combustion chamber. In this case, the liquid fuel does not always completely vaporize and mix before combustion occurs, resulting in persistent rich and lean pockets into which the turbulent flame propagates.

From a practical point of view, there are several basic and important issues regarding partially premixed combustion that need to be resolved. Two such issues are how reactant composition inhomogeneities affect the laminar and turbulent flame speeds, and how the burnt gas temperature varies as a function of these inhomogeneities. Knowledge of the flame speed is critical in optimizing combustion performance, and the minimization of pollutant emissions relies heavily on the temperature in the burnt gases. Another application of partially premixed combustion is found in the field of active control of turbulent combustion. One possible technique of active control consists of pulsating the fuel flow rate and thereby modulating the equivalence ratio (Bloxsidge *et al.* 1987). Models of partially premixed combustion would be extremely useful in addressing all these questions related to practical systems. Unfortunately, the lack of a fundamental understanding regarding partially

1 Institut de Mécanique des Fluides de Toulouse and CERFACS, France
2 Laboratoire EM2C, Ecole Centrale Paris, France
3 Institut Francais du Pétrole, France
4 Center for Turbulence Research

premixed combustion has resulted in an absence of models which accurately capture the complex nature of these flames.

Previous work on partially premixed combustion has focused primarily on laminar triple flames. Triple flames correspond to an extreme case where fuel and oxidizer are initially totally separated (Veynante *et al.* 1994 and Ruetsch *et al.* 1995). These flames have a nontrivial propagation speed and are believed to be a key element in the stabilization process of jet diffusion flames. Different theories have also been proposed in the literature to describe a turbulent flame propagating in a mixture with variable equivalence ratio (Müller *et al.* 1994), but few validations are available. The objective of the present study is to provide basic information on the effects of partial premixing in turbulent combustion. In the following, we use direct numerical simulations to study laminar and turbulent flame propagation with variable equivalence ratio.

2. Framework for analyzing and modeling partially premixed flames

Perfectly premixed combustion is usually described using a progress variable $c \equiv (Y_F^0 - Y_F)/(Y_F^0 - Y_F^1)$, where Y_F and Y_O are the fuel and oxidizer mass fractions, and the superscripts 0 and 1 refer to the values in the unburnt reactants and burnt products, respectively. Using the assumption of single-step chemistry and unity Lewis numbers, the progress variable provides a complete description of the transition from unburnt to burnt states and is the single relevant quantity used in model development and the postprocessing of simulation results. In partially premixed combustion, a new theoretical framework is required which will allow variable equivalence ratio along with simultaneous premixed and diffusion modes of combustion. This framework must use at least two scalar variables: one variable to describe the species composition, and a second variable to describe the progress of the premixed reaction. We use the mixture fraction Z as a description of the species composition, and a modified form of the progress variable c which accommodates the variable species composition in the fresh reactants.

We assume irreversible single step chemistry and unity Lewis numbers:

$$F + r_s(O + bN_2) \rightarrow P \tag{1}$$

where r_s is the stoichiometric oxidizer-fuel mass ratio and b is the N_2-O mass ratio, where N_2 is a diluent in the fresh reactants. The mixture fraction Z is then defined as:

$$Z \equiv \frac{(Y_F - Y_O/r_s + 1/(r_s(1+b))}{1 + 1/(r_s(1+b))}. \tag{2}$$

For stoichiometric mixtures, Z is equal to $Z_{st} = 1/(r_s(1+b)+1)$.* The fuel

* The equivalence ratio, $\phi \equiv r_s Y_F/Y_O$, is a more familiar quantity to the engineering community. However, ϕ and Z are simply related (Müller *et al.* 1994) through $\phi = Z(1 - Z_{st})/Z_{st}/(1-Z)$. We use Z rather than ϕ for the following reasons: ϕ is a conditional quantity that is only defined in the unburnt reactants whereas Z is not only defined everywhere in the flow, but is also conserved through the reaction, and Z is a linear combination of the species mass fractions and leads to straightforward expressions when averaging is employed.

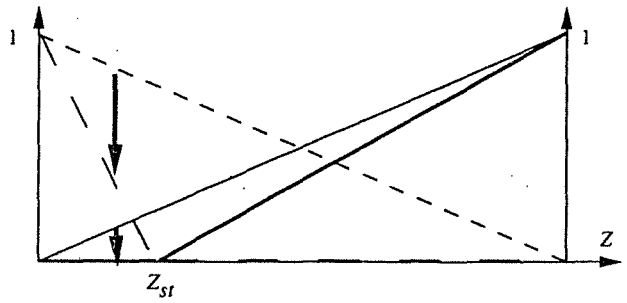

FIGURE 1. Fuel and oxidizer mass fractions as a function of the mixture fraction Z. ——— : Fuel Y_F^0/Y_F^∞ (mixing line) ; ---- : Oxidizer Y_O^0/Y_O^∞ (mixing line) ; ——— : Fuel Y_F^1/Y_F^∞ (fast chemistry line) ; — — — : Oxidizer Y_O^1/Y_O^∞ (fast chemistry line). The arrows indicate the transition from unburnt to burnt states in the case of perfectly premixed combustion, at a given equivalence ratio.

consumption rate, $\dot{\omega}_F$, and the heat release rate, $\dot{\omega}_T$, are written as:

$$\dot{\omega}_F = A\rho^p Y_F^n Y_O^m exp(-T_a/T) \quad \text{and} \quad \dot{\omega}_T = q\dot{\omega}_F \tag{3}$$

where A, p, n, m are model constants, ρ is the mass density, and q is the heat of reaction per unit mass of fuel. The activation temperature T_a is specified via a Zeldovich number, $\beta \equiv \alpha T_a/T_b(Z_{st})$, where α is the stoichiometric heat release factor, $\alpha \equiv (T_b(Z_{st}) - T_0)/T_b(Z_{st})$. The unburnt gas temperature, T_0, is assumed uniform in the present study, and the adiabatic flame temperature, $T_b(Z_{st})$, is calculated under stoichiometric conditions.

The mixture composition upstream of the flame zone is only a function of Z and may be described by the two mixing lines shown in Fig. 1 and given by

$$\frac{Y_F^0}{Y_F^\infty} = Z \quad \text{and} \quad \frac{Y_O^0}{Y_O^\infty} = 1 - Z \tag{4}$$

where the superscript ∞ denotes the value of the mass fraction in the respective feeding streams, such that $Y_F^\infty = 1$ and $Y_O^\infty = 1/(1+b)$.

If the chemistry is sufficiently fast, the mixture composition downstream of the premixed flame corresponds to the classical Burke-Schumann limit where fuel and oxidizer cannot coexist. This limit is a function of Z alone, and is sketched in Fig. 1 and given by

$$\frac{Y_F^1}{Y_F^\infty} = Max\left(0, \frac{Z - Z_{st}}{1 - Z_{st}}\right) \quad \text{and} \quad \frac{Y_O^1}{Y_O^\infty} = Max\left(0, 1 - \frac{Z}{Z_{st}}\right). \tag{5}$$

Premixed combustion changes the mixture composition from an unburnt state, as described by Eq. (4), to a burnt state, as described by Eq. (5). Under the flamelet assumption, this change occurs in a thin flame zone. Note that in perfectly premixed combustion, the mixture fraction Z is constant and the transition from unburnt to

burnt states occurs on a vertical line in Fig. 1. In partially premixed combustion, the transition may occur with simultaneous variations in Z.

Equations (4) and (5) lead to the following generalized definition of the premixed reaction progress variable:

$$c \equiv \frac{ZY_F^\infty - Y_F}{ZY_F^\infty - Max\left(0, \frac{Z-Z_{st}}{1-Z_{st}}\right) Y_F^\infty}. \tag{6}$$

For lean mixtures, where $Z \leq Z_{st}$ everywhere, we have

$$c = 1 - \frac{Y_F}{ZY_F^\infty} \tag{7}$$

and for rich mixtures, with $Z \geq Z_{st}$ everywhere, the following holds:

$$c = \frac{ZY_F^\infty - Y_F}{ZY_F^\infty - \left(\frac{Z-Z_{st}}{1-Z_{st}}\right) Y_F^\infty} = 1 - \frac{Y_O}{(1-Z)Y_O^\infty}. \tag{8}$$

If Z is constant, Eq. (6) reduces to the standard definition of c used in perfectly premixed combustion.

For the sake of simplicity, we now limit our discussion to the case of a lean mixture. A balance equation for c may be derived from basic conservation equations for the fuel mass fraction Y_F and for the mixture fraction Z:

$$\frac{\partial c}{\partial t} + u_i \frac{\partial c}{\partial x_i} = \frac{1}{\rho} \frac{\partial}{\partial x_k} \left(\rho D \frac{\partial c}{\partial x_k}\right) - \frac{\dot{\omega}_F}{\rho Z Y_F^\infty} + \frac{2D}{Z} \frac{\partial c}{\partial x_i} \frac{\partial Z}{\partial x_i} \tag{9}$$

where u_i is the fluid velocity and D is the mass diffusivity. This equation is similar to the one obtained in perfectly premixed combustion, except for the last term on the right-hand side. The sign of this additional term can be either positive or negative, suggesting flame propagation can either accelerate or decelerate as a result of partial premixing. Following Trouvé and Poinsot (1994), the conservation equation for c may be used to define the displacement speed of iso-c surface contours:

$$w(c = c^*) = \frac{1}{|\nabla c|} \left[\frac{\partial c}{\partial t} + u_i \frac{\partial c}{\partial x_i}\right] = \frac{1}{|\nabla c|} \left[\frac{1}{\rho} \nabla \cdot (\rho D \nabla c) - \frac{\dot{\omega}_F}{\rho Z Y_F^\infty} + \frac{2D}{Z} \nabla c \cdot \nabla Z\right] \tag{10}$$

where all quantities are evaluated at $c = c^*$. An alternative form of this equation is:

$$w = \frac{1}{|\nabla c|} \left[\frac{1}{\rho} \nabla \cdot (\rho D \nabla c) - \frac{\dot{\omega}_F}{\rho Z Y_F^\infty}\right] - \frac{2D}{Z} \boldsymbol{n} \cdot \nabla Z \tag{11}$$

where $\boldsymbol{n}$ is the local unit vector normal to the iso-c surface, $\boldsymbol{n} \equiv -\nabla c / |\nabla c|$. Adopting a flamelet point of view, we identify the thin flame surface as an iso-c surface with $c^* = 0.8$. Equation (11) can then be interpreted as an expression for the flame

propagation speed. The terms within brackets on the right-hand side of Eq. (11) show the dependence of the flame propagation speed on the local mixture fraction Z. The last term on the right-hand side shows the dependence of the flame propagation speed on the local Z-gradient normal to the flame. Hence, one basic effect of incomplete reactant mixing is the modification of the local flame speed, $w(Z, \boldsymbol{n} \cdot \nabla Z)$.

We now discuss the implications of partial premixing in the framework of flamelet combustion. In the flamelet picture, the mean reaction rate may be written as the product of a mean mass burning rate times the flame surface density:

$$\langle \dot{\omega}_F \rangle = \langle \dot{m} \rangle_S \Sigma \tag{12}$$

where $\dot{m}$ is the local mass burning rate per unit flame surface area, $\dot{m} = \int_n \dot{\omega}_F dn$, and Σ is the mean flame surface-to-volume ratio (the flame surface density). The operator $\langle \rangle_S$ denotes a flame surface average (Pope 1988).

Partial premixing can induce modifications of the mean reaction rate through several mechanisms: a modification of the local flame structure and corresponding modifications to the mean mass burning rate $\langle \dot{m} \rangle_S$, and contributions to the flame wrinkling resulting in a modification to the flame surface density Σ. The effect of partial premixing on flame wrinkling may be analyzed by considering the exact balance equation for Σ (Pope 1988, Candel & Poinsot 1990, Trouvé & Poinsot 1994):

$$\frac{\partial \Sigma}{\partial t} + \nabla \cdot \langle \mathbf{u} \rangle_S \Sigma + \nabla \cdot \langle w \mathbf{n} \rangle_S \Sigma = \langle \kappa \rangle_S \, \Sigma = \langle \nabla \cdot \boldsymbol{u} - \boldsymbol{n}\boldsymbol{n} : \nabla \boldsymbol{u} \rangle_S \, \Sigma + \langle w \nabla \cdot \boldsymbol{n} \rangle_S \, \Sigma \tag{13}$$

where κ is the flame stretch, which is decomposed in Eq. (13) into a production term due to hydrodynamic straining and a production or dissipation term due to flame propagation. The propagation term is the mean product of the local flame propagation speed, w, times the local flame surface curvature, $\nabla \cdot \boldsymbol{n}$. Hence, the effect of partial premixing on the local flame speed, $w(Z, \boldsymbol{n} \cdot \nabla Z)$, as seen in Eq. (11), can be interpreted as an effect of partial premixing on flame stretch, $\kappa(Z, \boldsymbol{n} \cdot \nabla Z)$, and thereby an effect on Σ. One objective of the present study is to determine the relative weight of effects induced by partial premixing on Σ and $\langle \dot{m} \rangle_S$ relative to the effects of turbulence on these quantities.

3. Numerical configurations and diagnostics

In the present study, one-, two-, and three-dimensional direct numerical simulations are performed with variable density and simple chemistry. The simulations use a modified Padé scheme for spatial differentiation that is sixth-order accurate (Lele 1992), a third-order Runge-Kutta method for temporal differentiation, and boundary conditions specified with the Navier Stokes characteristic boundary condition procedure (Poinsot & Lele 1992). We refer the reader to the Proceedings of the 1990, 1992, and 1994 CTR Summer Programs for further details concerning the system of equations solved and the numerical methods.

CONFIGURATION	FLOW	Z distribution (Lean=L Rich=R)
1/ x-inhomogeneous 1D unsteady flame	LAMINAR	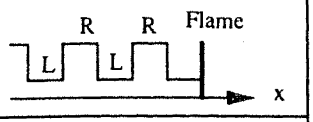
2/ y-inhomogeneous 2D steady flame	LAMINAR	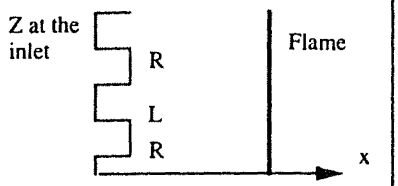
3/ xy-inhomogeneous 2D unsteady flame	LAMINAR	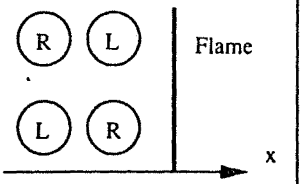
4/ xyz 3D flame	TURBULENT	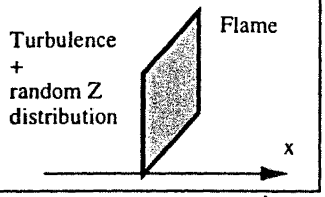

FIGURE 2. Configurations for DNS of partially premixed flames

The numerical configuration corresponds to a premixed flame propagating into a mixture with variable equivalence ratio. The mixture composition upstream of the flame is specified according to the probability density function, an integral length scale of the scalar field, and the relevant directions of inhomogeneity. The probability density function of Z is denoted as $p(Z)$ and can be characterized by its mean and rms values, $\langle Z \rangle$ and Z'. The amplitude of the fluctuations, ΔZ, can be used in place of the rms fluctuation for laminar cases. The characteristic integral length scale of the Z-field is denoted as l_Z. The directions of inhomogeneity in the Z-field are compared to the mean flame front orientation. We choose the direction of mean flame propagation as the x-direction. A numerical configuration is called x-inhomogeneous if gradients of Z exist in the x-direction, the direction normal to the mean flame front. Likewise, a $y-$inhomogeneous configuration corresponds to a case where species gradients exist tangent to the mean flame front. A fully turbulent three-dimensional configuration is called xyz-inhomogeneous.

Four different configurations are pursued in this study, as depicted in Fig. 2: Case 1 is a one-dimensional, x-inhomogeneous, unsteady, laminar flame, with a double-peak Z-pdf; Case 2 is a two-dimensional, y-inhomogeneous, steady, laminar flame,

with a double-peak Z-pdf; Case 3 is a two-dimensional, xy-inhomogeneous, unsteady, laminar flame, with a triple-peak Z-pdf; and Case 4 is a three-dimensional, xyz-inhomogeneous, non-stationary, turbulent flame, with a Guassian Z-pdf. These configurations each have a slightly different simple chemistry scheme, as summarized in Table I. Case 4 corresponds to a single step reaction mechanism proposed by Westbrook & Dryer (1981) for C_3H_8-air combustion.

Table I. Parameters for the four simulation configurations.

Case	Dim	b	r_s	Z_{st}	p	n	m	β	α
1	1D	0	1	0.5	1	1	1	8	0.75
2	2D	0	1	0.5	2	1	1	8	0.75
3	2D	0	1	0.5	1	1	1	8	0.75
4	3D	3.29	3.64	0.06	1.75	0.1	1.65	8	0.75

In all cases we characterize the effects of partial premixing by comparing the results to those obtained with perfect premixing in the same configuration. The effects of partial premixing on the local flame structure are characterized by the mass burning rates:

$$r \equiv \frac{\dot{m}}{\dot{m}(Z_{st})} \quad \text{and} \quad r' \equiv \frac{\dot{m}}{\dot{m}(\langle Z \rangle)} \tag{14}$$

where the unprimed quantity uses the stoichiometric homogeneous laminar flame as a reference, whereas the primed quantity uses the homogeneous laminar flame with $Z = \langle Z \rangle$. The global effects of partial premixing are characterized by the total reaction rate ratios:

$$R \equiv \frac{\Omega}{\Omega_0(Z_{st})} \quad \text{and} \quad R' \equiv \frac{\Omega}{\Omega_0(\langle Z \rangle)} \tag{15}$$

where $\Omega \equiv \int_V \langle \dot{\omega}_F \rangle dV$, with Ω_0 corresponding to a homogeneous, planar, laminar flame. These total reaction rate ratios can be rewritten as:

$$R = \frac{\int \langle r \rangle_S \Sigma dV}{\int \Sigma dV} \frac{\langle S_V \rangle}{S_0} \cdot \text{and} \quad R' = \frac{\int \langle r' \rangle_S \Sigma dV}{\int \Sigma dV} \frac{\langle S_V \rangle}{S_0} \tag{16}$$

where S_V is the total flame surface area within V, and S_0 is the projected area of the flame on a surface perpendicular to the direction of mean propagation. The first ratio in these expressions for R and R' accounts for modifications of the mean mass burning rate due to partial premixing, and the second ratio accounts for flame surface wrinkling due to turbulence and partial premixing. We write $W \equiv S_V/S_0$ and $\widehat{r'} \equiv \int \langle r' \rangle_S \Sigma dV / \int \Sigma dV$. The effects of partial premixing on flame temperatures are characterized by the following temperature ratios:

$$\theta \equiv \frac{T_{max} - T_0}{T_{max,0}(Z_{st}) - T_0} \quad \text{and} \quad \theta' \equiv \frac{T_{max} - T_0}{T_{max,0}(\langle Z \rangle) - T_0} \tag{17}$$

where $T_{max,0}$ corresponds to the case of a homogeneous, planar, laminar flame.

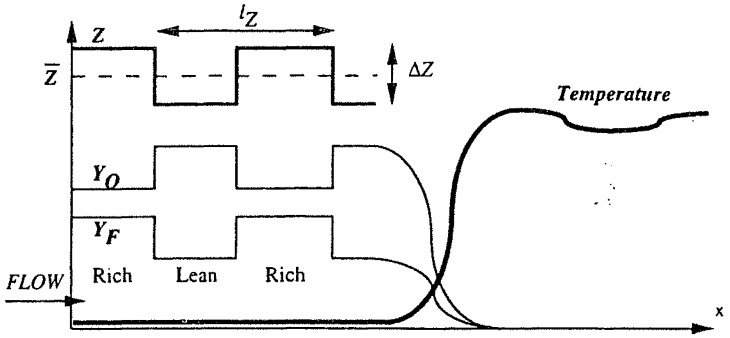

FIGURE 3. Case 1: One-dimensional, x-inhomogeneous, unsteady, laminar flames

4. Case 1: One-dimensional, x-inhomogeneous, unsteady, laminar flames

In this case, the inhomogeneity of reactant species is longitudinal with respect to the flow, and thus the flame response to temporal fluctuations in the mixture composition is studied. The mixture composition is forced at the inlet of the computational domain in order to generate harmonic perturbations in the Z-field upstream of the flame. These perturbations in Z are characterized by their mean value, $\langle Z \rangle$, their amplitude, ΔZ, and their wavelength l_Z (see Fig. 3). This case is well-suited to bring basic information on both flame structure modification and quenching by partial premixing.

In order to study the flammability limits of partially premixed flames, it is important to determine whether the simplified kinetic scheme used in the simulation is capable of reproducing realistic variations of the laminar flame speed, S_L, when variations occur in the mixture composition or equivalence ratio, ϕ. In particular, the lean and rich flammability limits must be correctly predicted. The single-step chemistry model presented in Section 2 does not have this capability unless heat losses are added to the energy equation. The choice of a nonadiabatic flame may be viewed as a simple fix to produce realistic variations $S_L(\phi)$, which is presented in Fig. 4. Following Williams (1985), we use a volumetric heat loss term $\mathcal{L}$ that is linear in $(T - T_0)$ (see also Poinsot *et al.* 1991):

$$\mathcal{L} = \frac{h}{\beta} \tau \rho_0 \frac{S_L(Z_{st})^2}{D_{th}} C_p T_0 \frac{\alpha}{1-\alpha} \tag{18}$$

where h is a model constant, chosen as $h = 0.031$, and $\tau \equiv (T - T_0)/(T_b(Z_{st}) - T_0)$.

As seen in Fig. 4, no abrupt transition to extinction is observed for the adiabatic single-step chemistry model, where very lean and very rich mixtures continue to burn. As a result, flame speeds are unrealistically high in these lean and rich regions. However, a domain of flammability is obtained using nonadiabatic single-step chemistry. This domain compares reasonably well to computations performed with a detailed mechanism proposed by Westbrook & Dryer (1981), for CH_4-air flames. While the prediction of the rich flammability limit is overestimated, the overall level of accuracy is deemed acceptable at the present stage.

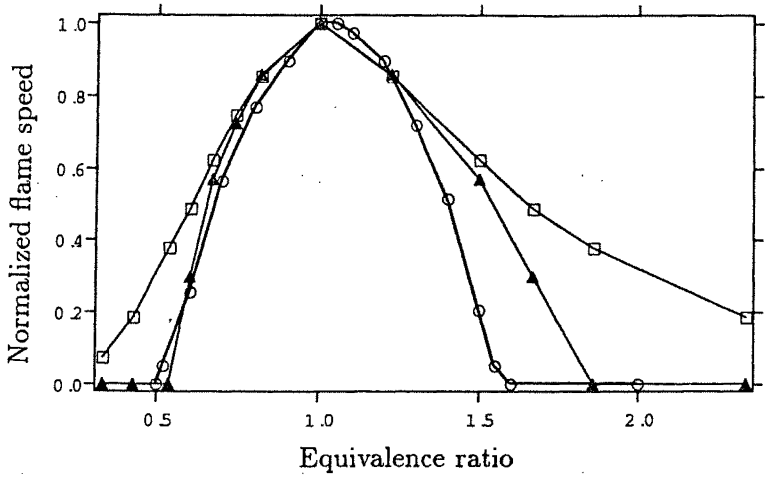

FIGURE 4. Variations of normalized flame speed with equivalence ratio, $s(\phi)$, for a one-dimensional, homogeneous, laminar flame. □ : Adiabatic one-step chemistry; ▲ : Non-adiabatic one-step chemistry; o : Detailed mechanism.

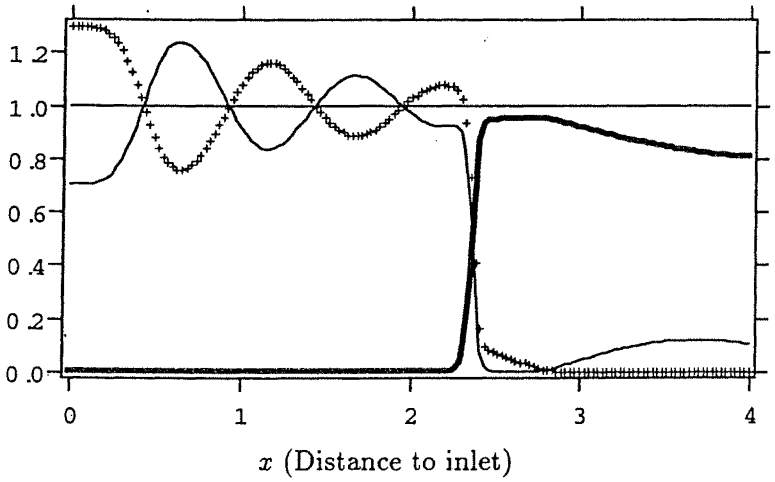

FIGURE 5. Case 1 with $\langle Z \rangle = Z_{st} = 0.5$, $\Delta Z = 0.2$ (at inlet), and $l_Z/\delta_L^0 = 14$, where δ_L^0 is the thermal thickness of the perfectly premixed flame with $Z = \langle Z \rangle$. + : Reduced Y_f ; —— : Reduced Y_O ; —— : Reduced temperature τ.

Figure 5 presents a typical snapshot of Y_F, Y_O, and temperature profiles across the flame zone. Species mass fractions are normalized in this figure by their stoichiometric values. One difficulty in these low Reynolds number simulations is that the perturbations in Z imposed at the inlet are strongly affected by molecular diffusion and are significantly damped before they reach the flame. In this situation, the flame response has the undesirable feature of depending on the flame location inside the computational domain. Nevertheless, we feel that the present simulations

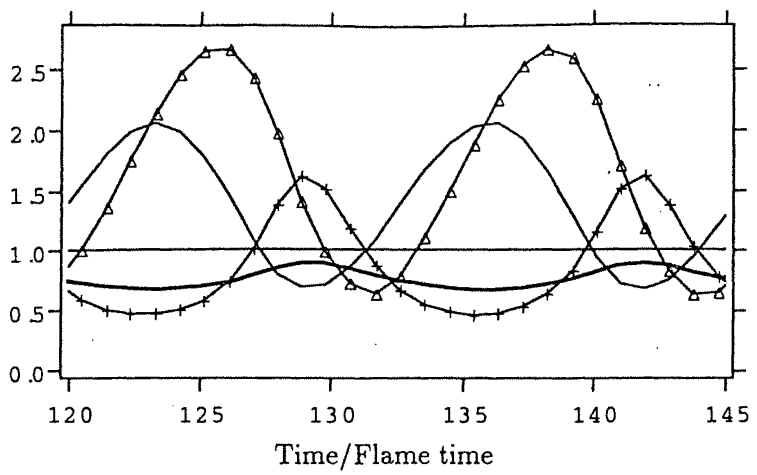

FIGURE 6. Case 1 with $\langle Z \rangle = 0.4$, $\Delta Z = 0.2$ (at inlet), and $l_Z/\delta_L^0 = 11$, where δ_L^0 is the thermal thickness of the perfectly premixed flame with $Z = \langle Z \rangle$. ——— : reduced flame thickness ; ——— : reduced maximum temperature θ' ; + : reduced flame speed r' ; $\triangle$: flame distance to inlet.

can still be used to describe the basic features of partially premixed flames.

The example presented in Fig. 5 corresponds to a perturbation in Z with alternative fuel rich ($Z \geq Z_{st}$) and fuel lean ($Z \leq Z_{st}$) pockets. The excess fuel and excess oxidizer that are not consumed by the premixed flame will burn in a diffusion flame. The intensity of this post-diffusion flame is rather low and in the case of Fig. 5, some unburnt fuel is found at the outlet of the computational domain. In a similar simulation, but with $\langle Z \rangle = 0.45$, there is no leakage of fuel.

Figure 6 presents typical time variations of the different diagnostics used to characterize the flame response. When the flame meets a pocket with a mixture composition close to stoichiometry, the flame speed and temperature increase, the flame thickness decreases, and the flame moves upstream in the computational domain. The converse is true when a pocket of mixture composition further from stoichiometry reaches the flame. Variations in flame speeds are large, with $0.5 < r' < 1.5$, and show deviations from a sinusoidal evolution: the time required for the flame to cross a given constant-Z pocket increases as Z moves away from stoichiometric conditions. This bias accounts for a reduced overall mean combustion rate compared to the perfectly premixed case, thus $R' < 1$.

Depending on the values of $\langle Z \rangle$, ΔZ, and l_Z, the effect of partial premixing on the mean reaction rate can either be positive, with $R' > 1$, or negative, with $R' < 1$. Figures 7 and 8 show that this effect remains weak, however, except for conditions close to the flammability limit. In Fig. 7, mixtures with $\Delta Z = 0.2$, and $\langle Z \rangle$ below 0.38 are quenched, while they would burn if perfectly premixed ($\Delta Z = 0.0$). Similarly, in Fig. 8 mixtures with $\Delta Z = 0.2$, $\langle Z \rangle = 0.4$, and $l_Z/\delta_L^0 > 14$ are quenched while they would burn if perfectly premixed. Fig. 8 also shows a comparison between the adiabatic and nonadiabatic simulations. Differences are

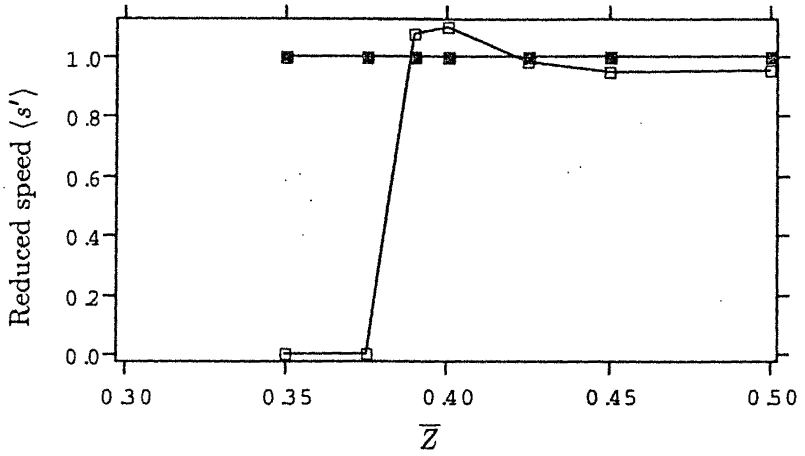

FIGURE 7. Case 1 with variable $\langle Z \rangle$. □ : R' (reduced overall mean combustion rate) in partially premixed flames ($\Delta Z = 0.2$ at inlet) ; ■ : R' in perfectly premixed flames ($\Delta Z = 0.$).

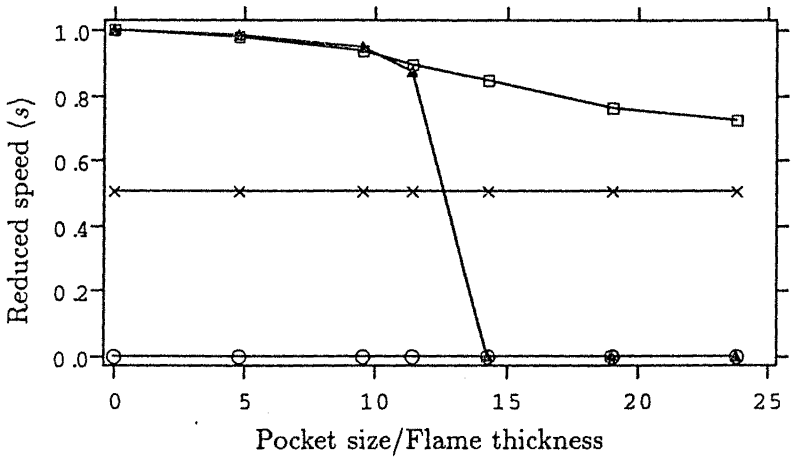

FIGURE 8. Case 1 with variable l_Z, $\langle Z \rangle = 0.4$, and $\Delta Z = 0.2$ (at inlet). □ : R (reduced overall mean combustion rate) in adiabatic flames ; ▲ : R in non-adiabatic flames ; × : asymptotic value S_a for adiabatic flames ; ○ : asymptotic value S_a for non-adiabatic flames.

small until transition to extinction is observed in the non-adiabatic case. In both cases, as l_Z becomes very large, the mean flame speed tends to an asymptotic value S_a given by the following expression:

$$S_a = \frac{2}{\frac{1}{S_L^-} + \frac{1}{S_L^+}} \tag{19}$$

where $S_L^- = S_L(\langle Z \rangle - \Delta Z/2)$ and $S_L^+ = S_L(\langle Z \rangle + \Delta Z/2)$. In Fig. 8, without heat

loss, $S_a/S_L(Z_{st}) = 0.51$; with heat loss, $S_a = 0$.

In summary, partial premixing in the one-dimensional case leads to strong temporal variations of the laminar flame structure, and in particular to strong fluctuations in the instantaneous values of the flame speed S_L and the mass burning rate $\dot{m}$. In the absence of quenching, these variations tend to cancel in the mean, and $\langle S_L \rangle$ and $\langle \dot{m} \rangle$ remain close to the values of S_L and $\dot{m}$ obtained in perfectly premixed systems. However, quenching induced by partial premixing has been observed in the case of strong variations in mixture composition, characterized by large amplitudes of $\Delta Z > 0.2$, or large length scales of $l_Z/\delta_L^0 > 10$.

5. Case 2: Two-dimensional, y-inhomogeneous, steady, laminar flames

In this configuration, inhomogeneities in the reactant species exist in the direction tangent to the flame, allowing the solution to converge to a steady state. This configuration is depicted in Figure 2, where the mixture fraction at the inlet is given by:

$$Z = \langle Z \rangle - \frac{\Delta Z}{2} \cos\left(\frac{2\pi y}{l_Z}\right)$$

For two dimensional flows, the parameter space becomes larger than the one-dimensional flows discussed previously, and we restrict ourselves to varying $\langle Z \rangle$ and ΔZ while maintaining l_Z constant. As these parameters are varied, we expect both the flame structure and propagation speed to change. As a result, the flame can advance or recede out of the computational domain. To avoid this problem, the inlet velocity, which remains uniform, is adjusted to accommodate changes in the flame speed. This procedure has been used in partially premixed combustion (Ruetsch *et al.* 1995 and Ruetsch and Broadwell 1995) and results in a steady-state configuration. This allows a well defined flame speed to be assessed in each run. Note that by defining the flame speed as the inlet velocity required to reach a steady state, we are considering a displacement speed.

As in the one-dimensional case, the mixture fraction is greatly modified from the time it is specified at the inlet to the time it reaches the flame. The range in mixture fraction at the flame surface is affected by several phenomena, including diffusion and the strain induced by the flame. Strain does not directly affect the mixture fraction, but does so implicitly by modifying the mixture fraction gradient in the lateral direction, which alters mass diffusion. The range of mixture fraction on the flame surface for all cases is shown in Fig. 9 as a function of the average mixture fraction. In addition to the reduction in mixture fraction range, the minimum and maximum values are no longer centered around the average value of the mixture fraction. The reason for this asymmetry becomes clear when we examine the structure of the flames when exposed to gradients in the mixture fraction.

5.1 Flame structure

The reaction rates and streamlines for flames subjected to different levels of $\langle Z \rangle$ are displayed in Fig. 10. For $\langle Z \rangle = Z_{ST} = 0.5$, we observe two leading edge flames within the domain. Since $\langle Z \rangle$ is at the stoichiometric value, we expect two equidistant leading edge flames and two equidistant troughs. As we decrease $\langle Z \rangle$ from the

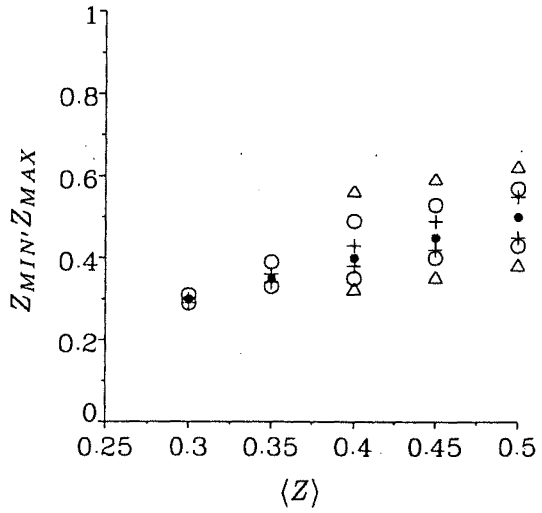

FIGURE 9. Range in mixture fraction on flame surface as a function of $\langle Z \rangle$. The different symbols correspond to different values of ΔZ at the inlet according to the following: • represents the homogeneous case ($\Delta Z = 0$ at inlet), + represents $\Delta Z = 0.2$, ○ represents $\Delta Z = 0.4$, and △ represents $\Delta Z = 0.8$. For the chemical scheme used in this case, $Z_{ST} = 0.5$.

stoichiometric value, this symmetry no longer exists. For the case with $\langle Z \rangle = 0.45$, we still have two stoichiometric points on the flame surface, although they have moved closer together. For the other cases of $\langle Z \rangle = 0.4$ and 0.35, stoichiometric points no longer exist on the flame surface. In these cases, the leading edge is located where the mixture fraction is closest to the stoichiometric value.

The reason for the asymmetric nature of the minimum and maximum values of Z on the flame surface, as observed in Fig. 9, can be easily understood from the flame shapes in Fig. 10. Diffusion of species has a longer time to act before reaching the flame surface the farther the flame is from the inlet. Therefore, the difference in mixture fraction along a horizontal line between the flame's leading edge and inlet is smaller than this difference along a line passing through the flame trough. For the case of $\langle Z \rangle = 0.5$, the maximum and minimum values of Z are both located in the troughs which occur at the same horizontal location, and we have symmetry in minimum and maximum values. As we depart from average stoichiometry, with $\langle Z \rangle < Z_{ST}$, the trough with rich composition moves forward and the lean trough backwards, so that diffusion has less time to act in the rich branch as compared to the lean branch. Therefore, the mixture fraction in the lean branch moves closer to stoichiometry.

Another factor that affects Z on the flame surface concerns the role strain plays on species diffusion. The divergence of streamlines in front of the leading edge reduces the mixture fraction gradient along the flame surface at that location, thus inhibiting diffusion. The opposite occurs in the flame trough, where the gradient in mixture fraction steepens due to the convergence of streamlines, accentuating the

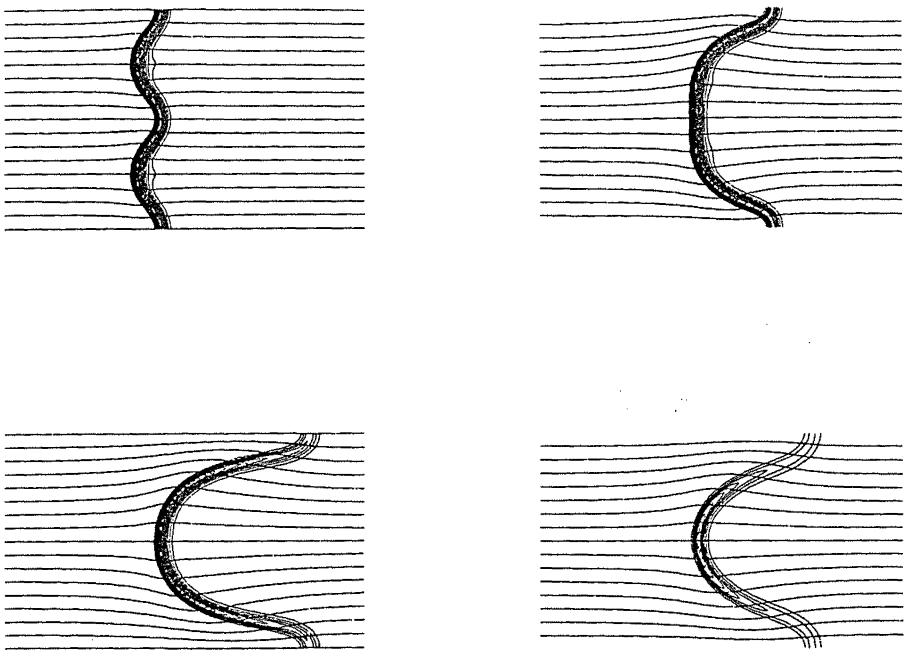

FIGURE 10. Contour plots or streamlines and reaction rates for simulations with $\Delta Z = 0.4$ and: $\langle Z \rangle = 0.5$ top left, $\langle Z \rangle = 0.45$ top right, $\langle Z \rangle = 0.4$ bottom left, and $\langle Z \rangle = 0.35$ bottom right.

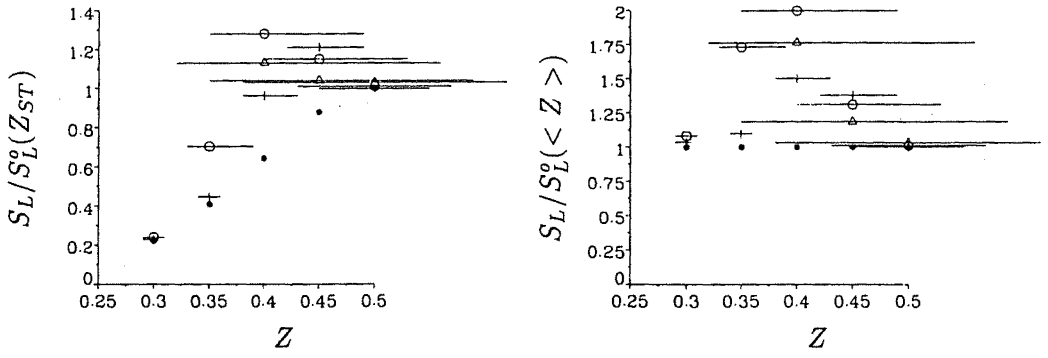

FIGURE 11. Propagation speed as a function of mixture fraction. The speeds are normalized by the homogeneous case at stoichiometric conditions, $S_L^0(Z_{ST})$, on the left, and by the homogeneous case at the average mixture fraction, $S_L^0(\langle Z \rangle)$ on the right. In addition to displaying the average mixture fraction of the run with the symbols, the range of mixture fraction on the flame surface is shown by the lines through each symbol. The legend for the symbols is provided in Fig. 9.

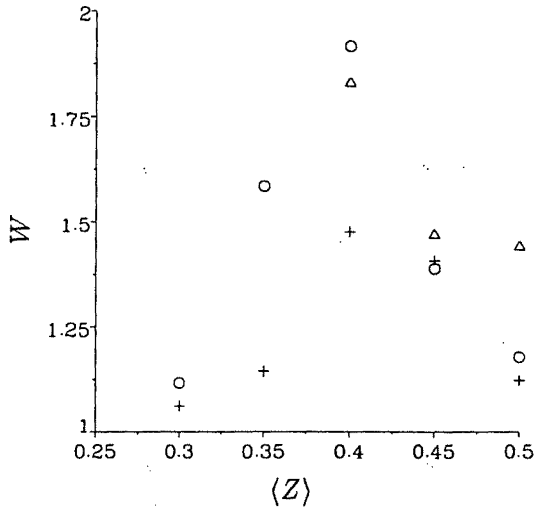

FIGURE 12. Flame wrinkling for the simulations. See Fig. 9 for a description of the symbols.

diffusion process.

As we progress towards lean mixture fractions to the point where stoichiometric conditions do not exist on the flame surface, the flame shape changes to the point where the spatial extent doubles, as the trough corresponding to rich mixture fractions disappears. This, in effect, alters the parameter l_Z without changing the computational domain. This doubling in lateral dimension has an effect on the flame speed as well as the flame shape, as is discussed in the next section.

5.2 Flame speed

When discussing the change in flame speed due to the inhomogeneous medium, it is useful to relate this displacement speed to that of the homogeneous case at both the average and stoichiometric mixture fractions, as shown in Fig. 11. In these figures, both the average mixture fraction at the inlet and the range of mixture fraction on the flame surface are shown by the symbols and lines, respectively. We begin discussion of the flame speed examining what occurs when the average composition is stoichiometric. Independent of the range in mixture fraction at the flame surface, the propagation speed remains that of the homogeneous case. This behavior was previously observed (Ruetsch and Broadwell 1995) when studying confined flames. For this value of l_Z, the lateral divergence of streamlines due to heat release is greatly inhibited by the confinement, and therefore the heat release mechanism responsible for enhanced flame speeds, as in the case of triple flames (Ruetsch and Broadwell 1995), is absent. As we depart from stoichiometry in the mean, the flame shape changes, effectively doubling l_Z, and we quickly move into a regime where streamline divergence is much stronger in front of the leading edge. An increase in flame speed is observed relative to $S_L(\langle Z \rangle)$, and in some cases even relative to $S_L^0(Z_{ST})$. It is interesting to note that flames with lean compositions

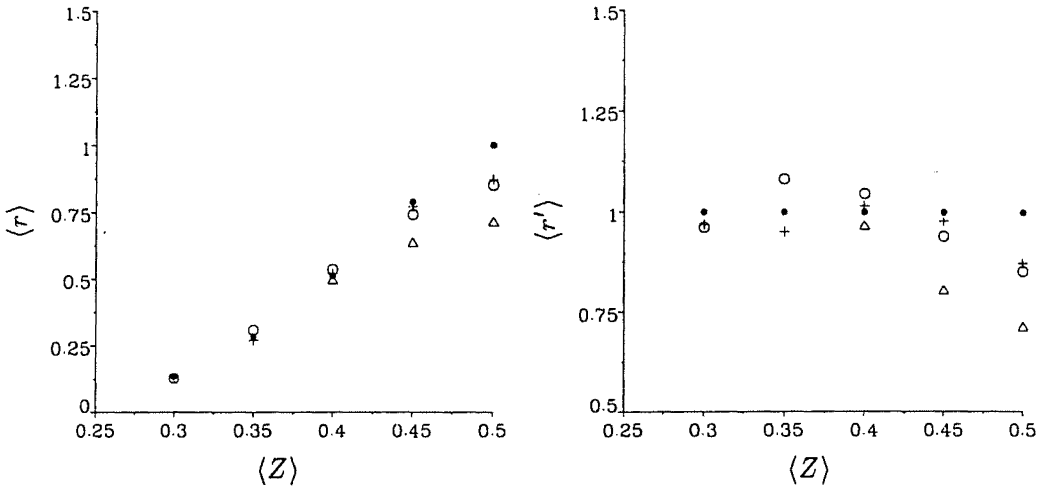

FIGURE 13. Average local reaction rate along flame surface normalized by the homogeneous case at Z_{ST} (left) and $\langle Z \rangle$ (right), as a function of the average mixture fraction.

along the entire length of the flame, designated in Fig. 11 by lines that do not cross $Z = Z_{ST} = 0.5$, can achieve flame speeds greater than the homogeneous stoichiometric case.

As $\langle Z \rangle$ further decreases, the reduction in reaction rate along the flame intensifies, and in spite of the streamline divergence the flame speed drops. As the flame speed drops, and along with it the inlet velocity in order to stabilize the flame in the computational domain, the mixture has a longer time to laterally diffuse as it approaches the flame. It is for this reason that the small range in mixture fraction at the flame surface is observed for very lean mixtures, apparent from Fig. 9, and is why the flame speed collapses to the homogeneous case.

Thus far we have concentrated on variations of flame speed with the average mixture fraction. We now turn our attention to how the fluctuation in mixture fraction about the mean affects the flame speed. As we have already mentioned, at mean stoichiometry the degree of inhomogeneity plays no role in flame speed. As the average mixture becomes lean, the flame speed increases as long as the composition at the leading edge stays near the stoichiometric value. For flames where the composition along the surface is always lean, the greatest speeds in absolute terms occur when the range in mixture fraction is the largest. This feature can be explained if we re-examine the flame structure. The streamline divergence depends on the flame curvature, which itself is determined by the local burning rate hence species composition. Therefore, the greatest range in mixture fraction along the surface would generate the greatest streamline divergence and increase in flame speed. This does not hold when the composition along the flame surface crosses stoichiometric values.

5.3 Fuel consumption

Having discussed the flame structure and propagation, we now turn our attention

to fuel consumption. Due to mass conservation, the global consumption rates given by R and R' are equivalent to the flame speed ratios shown in Fig. 11. There are slight discrepancies between the global reaction rate and flame speed ratios resulting from excess fuel leaving the domain in cases which have stoichiometric values on the flame surface. However, the domain is large enough, with a grid of $N_x = 361$ and $N_y = 121$, that almost all of the fuel is burned in either the premixed or diffusion modes before the flow exists the domain. We therefore use the flame speed ratios in Fig. 11 as R and R' in the following discussion.

For laminar flames we decompose the global burning rate in terms of the flame wrinkling, W, and the average burning rate along the flame surface, $\langle r \rangle_S$ or $\langle r' \rangle_S$, according to the following relations:

$$R = \langle r \rangle_S W; \qquad R' = \langle r' \rangle_S W. \tag{20}$$

The frame wrinkling is given in Fig. 12, and the mean reaction rates along the flame surface in Fig. 13. It is clear from Figs. 12 and 13 that flame wrinkling is the predominant factor in the global reaction rate modification.

The predominance of flame wrinkling over reaction zone modification is apparent for this steady-state configuration. We must now turn our attention to assessing whether this trend prevails when we consider flows with unsteadiness in both the scalar and flow fields. We address this issue for unsteady scalar fields in the following case, followed by a fully turbulent configuration.

6. Case 3: 2D, xy-inhomogeneous, unsteady, laminar flames

Case 3 includes two slightly different configurations, shown in Fig. 14. In Case 3a, the perturbations in Z correspond to an isolated pair of fuel lean and fuel rich pockets, whereas in Case 3b, the perturbations in Z correspond to an infinite array of such pockets. Case 3a provides basic information on the impulse response of a laminar flame subjected both to normal and tangential Z gradients, while Case 3b provides information on the response of a flame to periodic Z forcing. Table II gives the run parameters for the different simulations.

Table II. Simulation parameters for Case 3

Run	Case	$\langle Z \rangle$	ΔZ	$l_Z/\delta_L^0(\langle Z \rangle)$	h	N_x x N_y
A	3a	0.4	0.2	5.0	0.	127 x 127
B	3a	0.35	0.2	3.5	0.	127 x 127
C	3b	0.4	0.2	5.	0.	127 x 127
D	3b	0.35	0.2	3.5	0.	127 x 127
E	3b	0.3	0.2	1.9	0.	127 x 127
F	3a	0.4	0.2	5.0	0.031	127 x 127
G	3a	0.4	0.2	6.2	0.031	127 x 127

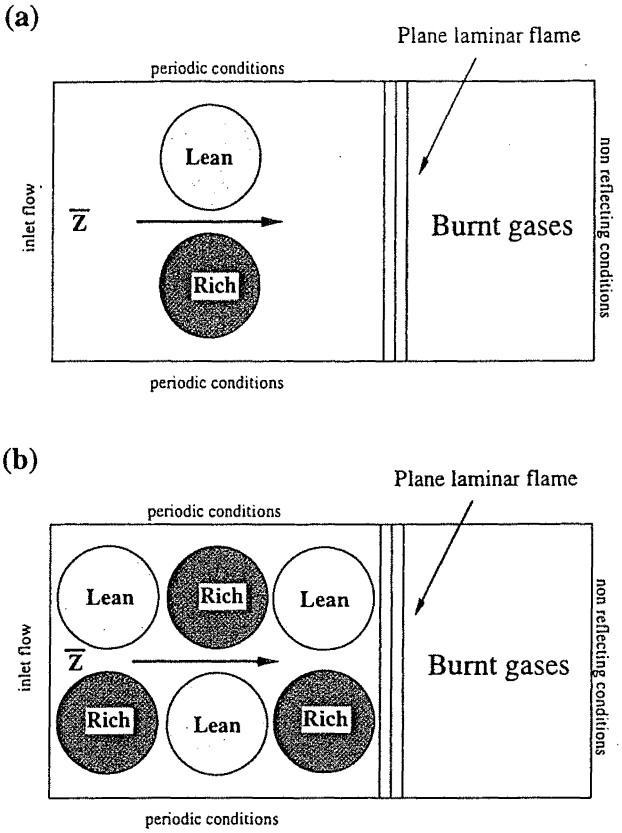

FIGURE 14. Case 3: Two-dimensional, xy-inhomogeneous, unsteady, laminar flames. (a) an isolated pair of lean ($Z = \langle Z \rangle - \Delta Z/2$) and rich ($Z = \langle Z \rangle + \Delta Z/2$) pockets, of size l_Z; (b) an infinite array of such pockets.

Figure 15 presents a typical snapshot of isocontours of $\dot{\omega}_F$, Z, c, and Y_P, as obtained in run A. Note that the generalized reaction progress variable defined in (7) is a good marker of the premixed flame front. Because it is affected by mixing within the burnt gases, Y_P is not a good choice to track the flame front. At the top of the figure, the flame is seen to interact with a fuel lean pocket ($Z = 0.3$), during which it decelerates and is convected downstream. At the bottom of the figure, the flame crosses a fuel rich pocket ($Z = Z_{st} = 0.5$), accelerates, and is convected upstream. These variations in the local flame displacement speed w correspond to strong variations in the local flame structure, as observed in Case 1. They also correspond to flame surface production.

As done in the steady-state situation of Case 2, we now compare the relative weight of the two basic effects of partial premixing as indicated in Eq. (20): the modification of the flame structure through $\langle r' \rangle_S$, and the generation of flame surface due to wrinkling, W. Figure 16 compares the temporal evolution of the relative contributions of these two terms to the global reaction rate from data obtained in

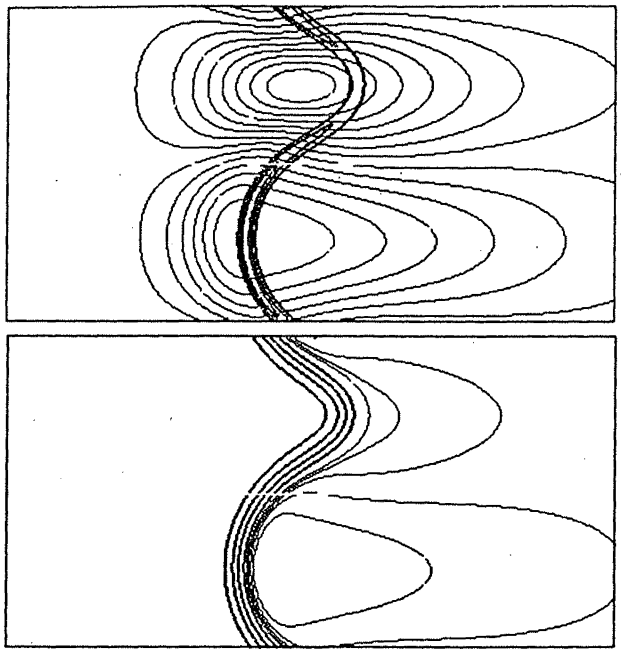

FIGURE 15. Case 3, run A, with $\langle Z \rangle = 0.4$, $\Delta Z = 0.2$, and $l_Z/\delta_L^0 = 5$. Top figure, isocontours of: reaction rate $\dot{\omega}_F$ (———) and mixture fraction Z (———). Bottom figure, isocontours of: reaction progress variable c (———) and product mass fraction Y_P (———).

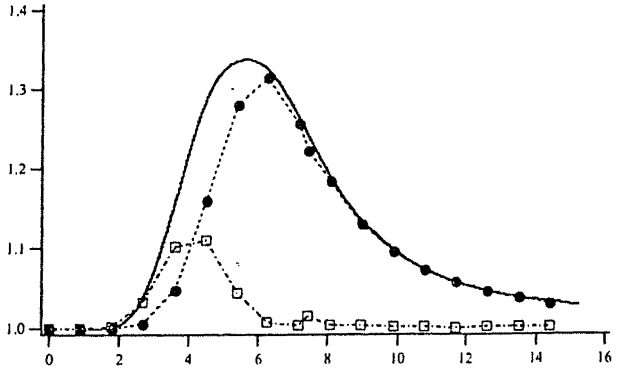

FIGURE 16. Case 3a, run A. Time evolution of the reduced global reaction rate R' (———), the reduced flame surface area W (•), and the reduced surface-averaged mass burning rate $\langle r' \rangle_S$ (□). Time is made non-dimensional by the laminar flame time $\delta_L^0(\langle Z \rangle)/S_L(\langle Z \rangle)$.

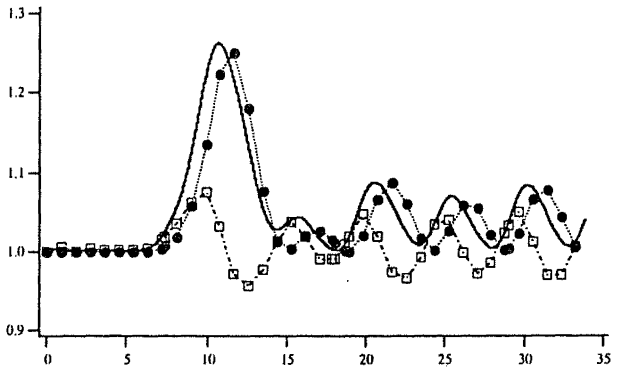

FIGURE 17. Case 3b, run C. Time evolution of the reduced global reaction rate R' (———), the reduced flame surface area W (•), and the reduced surface-averaged mass burning rate $\langle r' \rangle_S$ (□). Time is made nondimensional by the laminar flame time $\delta_L^0(\langle Z \rangle)/S_L(\langle Z \rangle)$.

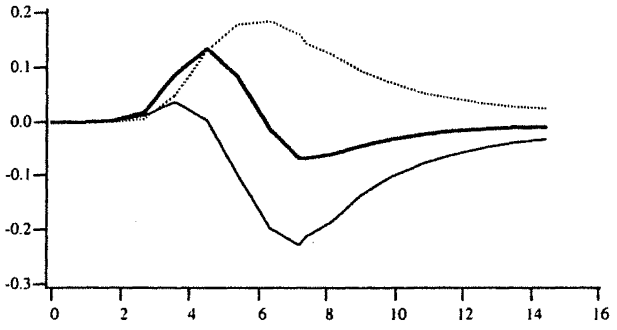

FIGURE 18. Case 3a, run A. Time evolution of the surface-averaged flame stretch $\langle \kappa \rangle_S$ (———), and its two components: the surface-averaged strain rate $\langle a_T \rangle_S$ (·····) and the surface-averaged propagation term $\langle w \nabla . \boldsymbol{n} \rangle_S$ (———). Time is made nondimensional by the laminar flame time $\delta_L^0(\langle Z \rangle)/S_L(\langle Z \rangle)$.

run A. Data from run A indicate behavior that is similar to the steady-state situation in Case 2. Partial premixing increases the global reaction rate, $R' > 1$, and the magnitude of the increase is typically 30-40%. The dominant effect of partial premixing is a production of flame surface area, $\langle r' \rangle_S \approx 1$ and $R' \approx W$.

Figure 17 presents similar results for run C. After an initial transient phase, the flame response reaches a limit cycle with periodic time-variations. At the limit cycle, the global reaction rate is increased compared to the perfectly premixed configuration, $R' > 1$; the magnitude of that increase is small, typically 10%; and this increase is related to flame surface production resulting from partial premixing $R' \approx W$.

As indicated by Eq. (13), the production of flame surface area is measured by flame stretch, and the surface-averaged flame stretch $\langle \kappa \rangle_S$ can be decomposed in

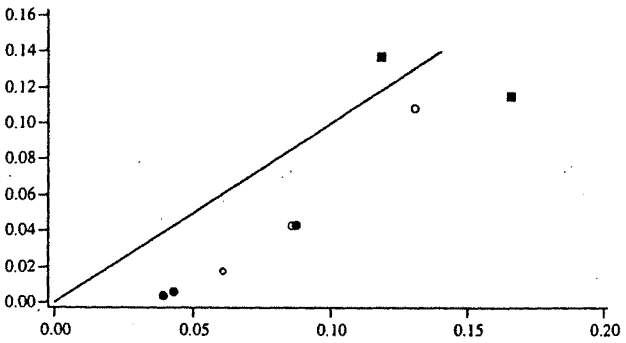

FIGURE 19. Test of Eq. (21): K_a^{PP} vs $(\Delta w/l_Z)(\delta_L^0/S_L(\langle Z\rangle))$. ○ Case 3a (runs A - B) ; • Case 3b (runs C - E); ▪ Case 3a with heat losses (runs F - G); ◇ A case with a single lean pocket.

a strain rate term, $\langle a_T\rangle_S = \langle \nabla.\boldsymbol{u} - \boldsymbol{nn} : \nabla\boldsymbol{u}\rangle_S$, and a propagation term, $\langle w\nabla.\boldsymbol{n}\rangle_S$. Figure 18 presents the temporal evolution of these two components of flame stretch and shows that partially premixed effects on stretch are not limited to the propagation term. A strong positive contribution of $\langle a_T\rangle_S$ is also observed. This contribution corresponds to a modification of the flow streamlines upstream of the curved flame, as observed in Fig. 10 for the steady configuration of Case 2.

It remains, however, that while the details of the temporal variations of $\langle\kappa\rangle_S$ depend on the effects of both hydrodynamic straining and flame propagation, the basic driving mechanism for flame surface production is the variation of the flame propagation speed w with mixture composition. A simple estimate of the global flame stretch induced by partial premixing may then be expressed as follows:

$$\kappa_{PP} \approx \frac{\Delta w}{l_Z} \tag{21}$$

where Δw is the amplitude of the variations of w measured at the flame location (due to molecular diffusion and unsteady effects, Δw is somewhat smaller than $S_L(\langle Z\rangle + \Delta Z/2) - S_L(\langle Z\rangle - \Delta Z/2)$), and l_Z is the size of the pocket. We use the peak value of $\langle\kappa\rangle_S$ observed in the flame's response to perturbations in Z to estimate the global flame stretch. In nondimensional form, we get the following estimate for a Karlovitz number induced by partial premixing:

$$K_a^{PP} \approx \frac{\Delta w}{l_Z}\frac{\delta_L^0(\langle Z\rangle)}{S_L(\langle Z\rangle)} \tag{22}$$

This relation is tested in Fig. 19 and is found to be satisfactory. Note, however, that the values of this Karlovitz number remain small, $K_a^{PP} \leq 0.2$.

In summary, partial premixing in Case 3 leads to both modification of the flame structure and production of flame surface area. In the absence of quenching, the dominant effect on the mean reaction rate is flame surface wrinkling, $R' \approx W$. It

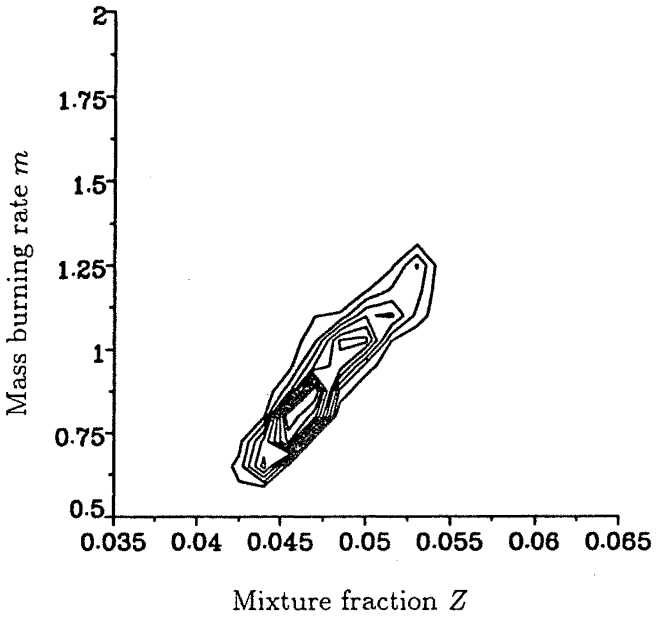

FIGURE 20. Case 4A. Joint probability density function of the reduced mass burning rate, r', and the flame mixture fraction, Z. Time $= 4l_t/u'$.

is always positive, $R' > 1$, but the magnitude of that effect as measured by an estimate of the partially premixed Karlovitz number remains small, $K_a^{PP} \leq 0.2$.

Table III. Initial conditions for Case 4 simulations

Case	$\langle\phi\rangle$	$\langle Z\rangle$	ϕ'	Z'	$l_Z/\delta_L^0(Z_{st})$	u'/S_L	$l_t/\delta_L^0(Z_{st})$	Re_t
4A	0.8	0.049	0.3	0.018	2	7.5	2	75
4B	0.8	0.049	0.3	0.018	2	2.5	2	25

7. Case 4: 3D, *xyz*-inhomogeneous, unsteady, turbulent flame

In this case, partial premixing effects are compared to those due to the turbulent motions. The numerical configuration corresponds to a premixed flame propagating into three-dimensional, decaying, isotropic turbulent flow, with variable equivalence ratio. We refer the reader to Trouvé & Poinsot (1994) for more information on the configuration, as well as the initial and boundary conditions. The new feature in the present simulations lies in the initialization of the scalar field in the flow of fresh reactants: Y_F, Y_O, and Y_{N2} are specified according to a model energy spectrum as proposed by Eswaran & Pope (1988). The initial probability distribution o equivalence ratio is a pdf with two peaks at $\phi = 0.5$ and $\phi = 1.1$. Because o turbulent mixing, this distribution quickly evolves to a Guassian pdf. Two differen

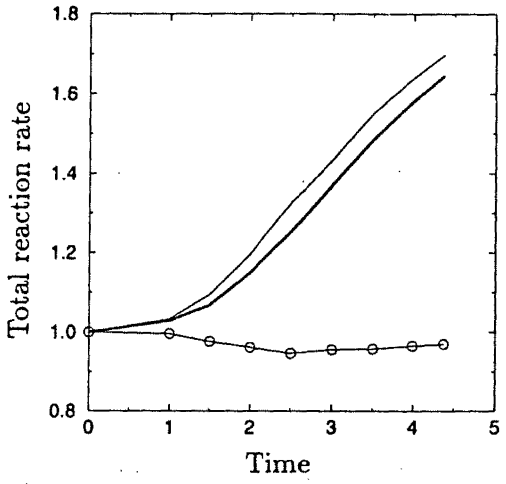

FIGURE 21. Case 4A. Time evolution of the reduced total reaction rate, R' (——), the reduced mean mass burning rate, $\widehat{r'}$ (o), and the reduced total flame surface area, $\langle W \rangle$ (——). Time is made non-dimensional by the initial, turbulent eddy turnover time, l_t/u'.

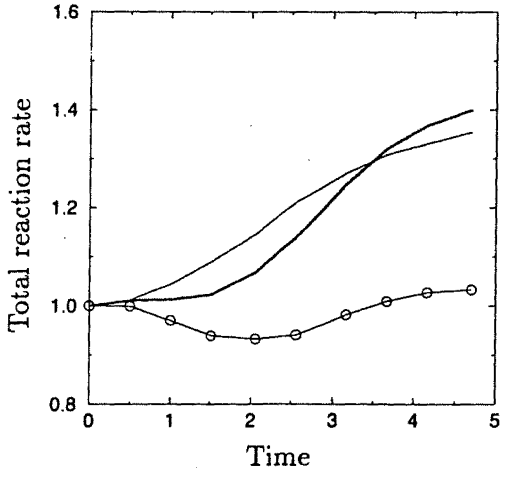

FIGURE 22. Case 4B. Time evolution of the reduced total reaction rate, R' (——), the reduced mean mass burning rate, $\widehat{r'}$ (o), and the reduced total flame surface area, $\langle W \rangle$ (——). Time is made non-dimensional by the initial, turbulent eddy turnover time, l_t/u'.

simulations were performed. The run parameters are given in Table III. In this table l_Z designates the integral length scale of the scalar field, u' the turbulent rms velocity, l_t the integral length scale of the velocity field, and Re_t the turbulent Reynolds number (based on u' and l_t). Cases 4A and 4B correspond to strongly and moderately turbulent flames, respectively. Also, the present simulations use the single step reaction mechanism proposed by Westbrook & Dryer (1981).

In the simulations, partial premixing results in strong spatial variations of the

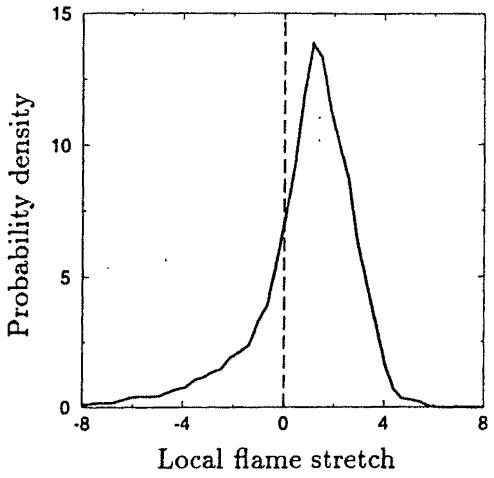

FIGURE 23. Case 4A. Probability density function of flame stretch, κ. Stretch is made non-dimensional by the laminar flame time $\delta_L^0(\langle Z\rangle)/S_L(\langle Z\rangle)$. Time $= 4l_t/u'$.

local combustion intensity along the turbulent flame front, consistent with the findings from the previous cases. In Fig. 20, this intensity is quantified by the reduced mass burning rate per unit flame surface area, r', where r' is seen to vary between 0.5 and 1.5. r' is also seen to correlate strongly with the local mixture composition, as measured by the flame mixture fraction. Interestingly, the correlation is approximately linear, so that departures of the mass burning rate $\dot{m}$ from the reference value $\dot{m}(\langle Z\rangle)$ (obtained from a homogeneous, planar, laminar flame) tend to cancel in the mean when averaged over the whole flame. This tendency is confirmed in Figs. 21 and 22, which present the temporal evolution of the two components of the total reaction rate, written for the turbulent case as:

$$R' = \widehat{r'}\langle W\rangle.$$

In Cases 4A and 4B, the mean mass burning rate remains within 10% of unity, so $\widehat{r'} \approx 1$, and the total reaction rate is approximately proportional to the flame surface area, $R' \approx \langle W\rangle$.

There are two mechanisms responsible for the production of flame area in these turbulent simulations: the interaction of the turbulent velocity field with the flame surface, and the partial premixing mechanism described in Cases 2 and 3. Eq. (21) can be used to determine the relative weight of these two mechanisms. The following nondimensional number gives an estimate of the ratio of stretch resulting from partially premixing to stretch due to the turbulent motion:

$$N_T \equiv \frac{\Delta w}{l_Z}\frac{l_t}{u'} = \frac{\Delta w}{S_L(\langle Z\rangle)}\frac{\delta_L^0(\langle Z\rangle)}{l_Z}\frac{l_t}{\delta_L^0(\langle Z\rangle)}\frac{S_L(\langle Z\rangle)}{u'} \tag{23}$$

where the turbulent stretch is estimated using the integral time scale of the turbulence. If $l_t \approx l_Z$, N_T may be further estimated as $(Z'/\langle Z\rangle)(S_L/u')$. Hence, N_T

scales as the inverse of the ratio of a characteristic turbulent flow velocity divided by a laminar flame velocity. N_T is likely to remain small in most practical situations. At the initial time, $N_T \approx 0.03$ in Case 4A; and $N_T \approx 0.1$ in Case 4B.

This last point is illustrated in Fig. 23. Figure 23 presents a typical probability distribution for flame stretch, as obtained in Case 4A. Stretch is normalized in Fig. 23 by a laminar flame time so that stretch values can be directly interpreted as values of the flame Karlovitz number, K_a. The simulation values of K_a range from -8 to 4. These values are quite large and the simulated flame is beyond the domain of possible stretch resulting from partial premixing, ($K_a^{PP} \leq 0.2$). Similar results are obtained in Case 4B.

In summary, partial premixing in the turbulent case leads to strong variations in the local flame mass burning rate, but these variations tend to average out, $\widehat{r'} \approx 1$. Due to the much larger values of turbulent stretch compared to partial premixing induced stretch, the production of flame surface area by partial premixing remains negligible, $N_T < 0.1$.

8. Conclusions

Direct numerical simulations of premixed flames propagating into laminar or turbulent flow, with variable equivalence ratio, are used in this paper to study the effects of partial premixing on the mean reaction rate. The flamelet theory is shown to provide a convenient framework to describe partially premixed flames.

Partial premixing leads to strong variations of the local flamelet structure, and in particular to strong variations of the mass burning rate per unit flame surface area, $\dot{m}$. In the absence of quenching, these variations tend to average out and the effect of partial premixing on the mean flamelet structure remains limited, $\langle \dot{m} \rangle_S \approx \dot{m}_L(\langle Z \rangle)$. Note, however, that quenching induced by partial premixing has been observed in the present simulations, in the case of strong variations in mixture composition, characterized by large amplitudes ($\Delta Z > 0.2$) or large length scales ($l_Z/\delta_L^0 > 10$).

Partial premixing induces flame stretch and, in the absence of quenching this effect, is dominant for laminar flames. It is always positive and will result, in the laminar case, in a partially premixed flame burning faster than the corresponding perfectly premixed flame. The magnitude of the effect of partial premixing on flame surface production is measured by Eq. (22). Typical values of the flame Karlovitz number are below 0.2, and this effect will be negligible in highly turbulent flames. This has been observed in the turbulent flames of this study, where wrinkling effects from partial premixing are small compared to wrinkling created by the fluid motion for the given initial conditions.

REFERENCES

BLOXSIDGE, G., DOWLING, A., HOOPER, N. & LANGHORNE, P. 1987 Active control of reheat buzz. *25th Aerospace Sciences Meeting.*

CANDEL, S. M. & POINSOT, T. 1990 Flame stretch and the balance equation for the flame surface area. *Combust. Sci. Tech.* **70,** 1-15.

ESWARAN, V. & POPE, S. B. 1988 Direct numerical simulations of the turbulent mixing of a passive scalar. *Phys. Fluids.* **31 (3),** 506-520.

HAWORTH, D. C. & POINSOT, T. J. 1992 Numerical simulations of Lewis number effects in turbulent premixed flames. *J. Fluid Mech.* **244,** 405-436.

LELE, S. 1992 Compact finite difference schemes with spectral like resolution. *J. Comput. Phys.* **103,** 16-42.

MÜLLER, C., BREITBACH, H. & PETERS, N. 1994 Partially premixed turbulent flame propagation in jet flames. *25th Symp. (Int.) Comb., The Combustion Institute.*

POINSOT, T., VEYNANTE, D. & CANDEL, S. 1991 Quenching processes and premixed turbulent combustion diagrams. *J. Fluid Mech.* **228,** 561-605.

POINSOT, T. & LELE, S. 1992 Boundary conditions for direct simulations of compressible viscous flows. *J. Comput. Phys.* **101,** 104-129.

POPE, S. 1988 The evolution of surfaces in turbulence. *Int. J. Engr. Sci.* **26,** 445-469.

RUETSCH, G. R., VERVISCH, L. & LIÑÁN, A. 1995 Effects of heat release on triple flames. *Phys. Fluids.* **7,** 1447.

RUETSCH, G. R. & BROADWELL, J. E. 1995 Effects of confinement on partially premixed flames. *Annual Research Briefs 1995.* Center for Turbulence Research, NASA Ames/Stanford University. 323-333.

TROUVÉ, A. & POINSOT, T. 1994 The evolution equation for the flame surface density. *J. Fluid Mech.* **278,** 1-31.

VEYNANTE, D., VERVISCH, L., POINSOT, T., LIÑÁN, A., & RUETSCH, G. R. 1994 Triple flame structure and diffusion flame stabilization. *Proceedings of the 1994 Summer Program.* Center for Turbulence Research, NASA Ames/Stanford University. 55-73.

WESTBROOK, C. & DRYER, F. 1981 Simplified Reaction Mechanism for the Oxidation of Hydrocarbon Fuels in Flames. *Combust. Sci. Tech.* **27,** 31-43.

WILLIAMS, F. A. *Combustion Theory.* Addison-Wessley, NY, 1986.